International Journal of Recent Engineering Research and Development (IJRERD)
ISSN: 2455-8761
www.ijrerd.com || Volume 11 – Issue 02 || Mar - Apr 2026 || PP. 41-52

# Modeling and Dynamic Simulation of an Automated Exercise Bed's Swing-Board Mechanism for Recuperating Patient

Dandakouta Habou[1], Amoo, Abdullahi Lanre[2] and Salawu Bashiru Ugonoh[3]
[1]*Department of Mechanical/Production Engineering, Abubakar Tafawa Balewa University Bauchi*
[2]*Department of Electrical and Electronics Engineering, Abubakar Tafawa Balewa University Bauchi*
[3]*Power Equipment and Electrical Machinery Development Institute (PEEMADI), Okene*

**Abstract:** This study aimed to dynamically model and optimize the swing-board mechanism of an automated exercise bed's swing-board mechanism for patient rehabilitation, addressing the global shortage of physiotherapists and the need for safe, autonomous therapy. Using a four-bar linkage configuration with initial dimensions of AB=150 mm, BC=400 mm, CD=350 mm, and AD=500 mm, the research applied Lagrangian mechanics and numerical simulation in MATLAB to derive motion equations and assess forces, velocities, and stresses. Optimized link lengths (AB=122 mm, BC=326 mm, CD=285 mm, AD=375 mm) produced a smooth vertical stroke of 0.463 m at 0.318 Hz, with peak velocity and acceleration kept below safety thresholds at 0.85 m/s and 3.2 m/s², respectively. Static and dynamic analyses using 6061 aluminum revealed a maximum von Mises stress of 28.45 MPa and safety factors between 9.7 and 15.2, ensuring structural integrity. The model demonstrated high energy conservation (ΔE=0.023 J/cycle) and periodicity (99.97% cycle match). Thestudyuniquely integrates dynamic optimization with therapeutic motion profiles, offering a cost-effective design alternative to imported systems. A limitation includes the assumption of idealized patient loading, thus further validation with human subjects is recommended.

**Keywords:** Automated rehabilitation, swing-board mechanism, four-bar linkage, Lagrange method, dynamic simulation, kinematic optimization, physiotherapy device.

## 1.0 Introduction

The global population aged over 60 is projected to reach 2.1 billion by 2050, significantly increasing the demand for post-operative and stroke rehabilitation services [1]. Stroke is a leading cause of adult disability, with a majority of survivors experiencing significant hemiparesis requiring long-term physiotherapy to regain functional mobility [2, 19]. The global shortage of physiotherapists, particularly in low-resource settings, exacerbates this challenge [3]. Automated rehabilitation systems, such as Continuous Passive Motion (CPM) machines, demonstrate proven efficacy, with studies showing improvements in range of motion exceeding 60% for specific joint therapies [3]. The COVID-19 pandemic further enforced the critical need for autonomous therapeutic solutions, as infection protocols limited hands-on care [4, 17]. This has accelerated research into rehabilitation robotics, including actuated beds and exoskeletons [5, 6, 19].

A significant research gap exists in the comprehensive dynamic modeling of the oscillatory mechanisms central to these systems. Many existing patient aids utilize simple linkages but are designed without rigorous dynamic analysis, leading to suboptimal motion profiles, patient discomfort, and potential mechanical failure under cyclic loading [7]. The dynamic response - including inertial forces, vibrations, and stress distributions; under realistic patient loads is often inadequately characterized, especially with varying health conditions of patients.

Computational modeling is paramount to addressing these limitations. The multi-body dynamics approach, particularly the Lagrange method, provides a powerful framework for deriving equations of motion for interconnected rigid bodies, allowing for the analysis of forces, torques, and displacements within mechanical systems [7]. This method is extensively used in robotics and vehicle dynamics but its application to medical device design, especially patient exercise mechanisms is inadequate, and thus, requires further exploration [8]. Recent studies have successfully applied Lagrange formalism to optimize the dynamics of robotic manipulators and exoskeletons, demonstrating reductions in peak actuator torque and energy consumption [9] However, a focused study on the swing board mechanisms of an automated bed, which must safely oscillate patient limbs with smooth, controlled motion [25], is lacking, resulting to lower performance, patient discomfort, and potential mechanical failure under cyclic loads. Many systems lack customized kinematic profiles tailored to specific therapeutic requirements for different body parts (head, arms, legs). Furthermore, the high cost of imported systems and a global shortage of physiotherapists limit accessibility, leaving a significant portion of the aging and recuperating population without adequate rehabilitation resources for the all-important physical exercises [5]. This work provides a multi-body dynamic model, using the

Lagrange method, to simulate and optimize the static and dynamic performance of a therapeutic mechanism, ensuring its efficacy, safety, and reliability before physical prototyping.

## 2.0 Methodology

The methodology for modeling and simulating the swing board mechanism was conducted in three sequential phases, namely: system configuration and kinematic modeling, dynamic formulation using the Lagrangian method, and numerical optimization with validation.

### 2.1 System Configuration and Kinematic Modeling

The oscillatory mechanism was conceptualized as a four-bar linkage, a proven standard configuration for generating controlled rhythmic motion [10]. A schematic diagram of the patient bed is shown in Figure 2.1(a) with head rest swing-board (1) and arm rest swing-board (2). The proposed four-bar swing-board mechanism for head and arm exercises is shown in Figure 2.1(b). It consists of a crank (link AB), coupler (link BC), rocker (link CD) - therapeutic swing board with an extended output link to accommodate varying sizes, and fixed ground link (link DA).

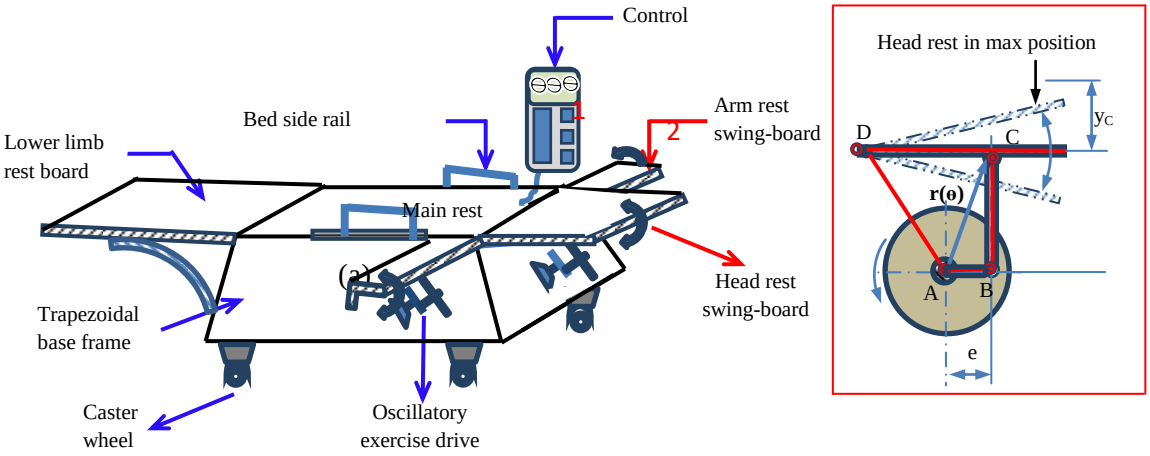


Figure 2.1: Schematic of the model concept for an automated patient bed for exercise
(a) bed assembly and (b) 4-bar link Mechanism the exercise board swings

The kinematic analyses were conducted to determine the position, velocity, and acceleration of the swing boards as a function of the crank angle, θ. The vector loop equation utilized for the linkage is given in Equation 1:

$$r_1 e^{i\theta_1} + r_2 e^{i\theta_2} = r_4 + r_3 e^{i\theta_3} \quad (1)$$

Separating into real and imaginary components provides Equations 2 and 3 as:

Real part: $r_1 \cos\theta_1 + r_2 \cos\theta_2 = r_4 + r_3 \cos\theta_3$ (2)

Imaginary part: $r_1 \sin\theta_1 + r_2 \sin\theta_2 = r_3 \sin\theta_3$ (3)

The coupler angle $\theta_2$ and rocker angle $\theta_3$ were solved using Freudenstein's equation derived from the loop closure conditions, as given in Equations 4 to 5.

$$\theta_2 = atan2(r_3 \cos\theta_3 - r_1 \sin\theta_1,\ r_4 + r_3 \cos\theta_3 - r_1 \cos\theta_1) \quad (4)$$

$$\theta_3 = \varphi \pm cos^{-1}\left(\frac{D}{R}\right) \quad (5)$$

Where: $D = \frac{r_2^2 - r_1^2 - r_3^2 - r_4^2}{2} + r_1 r_4 \cos\theta_1$, $R = \sqrt{E^2 + F^2}$, and $\varphi = atan2(F, E)$.

The transmission angle $\gamma$, an indicator of force transmission efficiency, is given by:

$$\gamma = \cos^{-1}\left[\frac{r_2^2 + r_3^2 - (r_1^2 + r_4^2 - 2r_1 r_4 \cos\theta_1)}{2r_2 r_3}\right] \quad (6)$$

The position of the board endpoint E, located at an extension L from point C, is:

$$x_E = r_1 \cos\theta_1 + r_2 \cos\theta_2 + L\cos\theta_3) \quad (7)$$

$$y_E = r_1 \sin\theta_1 + r_2 \sin\theta_2 + L\sin\theta_3) \quad (8)$$

Velocity and acceleration components were obtained by successive differentiation of the position equations 7 and 8 to give Equations 9 and 10:

$$v_{Ex} = -(r_3 + L)\dot{\theta}_3 \sin\theta_3 \quad (9)$$

$$v_{Ey} = (r_3 + L)\dot{\theta}_3 \cos\theta_3 \quad (10)$$

While the corresponding linear accelerations are given in Equations 11 and 12, as:

$$a_{Ex} = -(r_3 + L)\left(\ddot{\theta}_3 \sin\theta_3 + \dot{\theta}_3^2 \cos\theta_3\right) \quad (11)$$

$$a_{Ey} = (r_3 + L)\left(\ddot{\theta}_3 \cos\theta_3 - \dot{\theta}_3^2 \sin\theta_3\right) \quad (12)$$

The initial link dimensions assumed for a standard adult configuration were: crank AB = 150 mm, coupler BC = 400 mm, rocker CD = 350 mm, and fixed link AD = 500 mm, with a board extension CE = 200 mm.

**2.2 Dynamic Formulation using the Lagrangian Method**

The orientation of the link mechanism for dynamic analysis is shown in Figure 2.2, under the action of four different forces – inertia, gravity, damping and spring forces, giving the total force at point E which may be assumed to coincide with point C for now.

The generalized coordinate vector $\boldsymbol{q} = [\theta_1, \theta_2, \theta_3]^T$ was used to assemble the energy components of link mechanism in dynamic operation [23]. The total kinetic energy (KE) and potential energy (PE) of the system, accounting for all moving the links and the board mass, $m_b$ are:

$$KE = \frac{1}{2}\sum_{i=1}^{3}\left(m_i v_{Gi}^T v_{Gi} + I_i \dot{\theta}_i^2\right) + \frac{1}{2} m_b v_E^T v_E \quad (13)$$

$$PE = \sum_{1}^{3}(m_i g y_{Gi}) + m_b g y_E \quad (14)$$

where $m_i$ is the link mass, $I_i$ is the link moment of inertia, $v_{Gi}$ is the velocity of the center of mass, $k$ is the spring constant, and $y_{Gi}$ is the vertical position of the center of mass for link $i$, respectively.

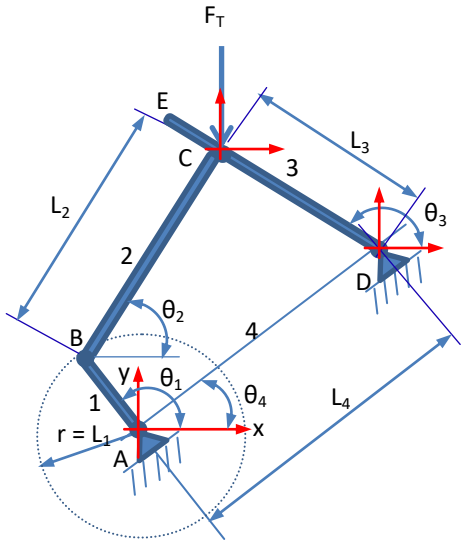


Figure 2.2: Four-bar link mechanism for Patient Recuperating Exercise

The Lagrangian $L = KE - PE$ is defined as:

$$\frac{d}{dt}\left(\frac{\partial L}{\partial \dot{\theta}_i}\right) - \frac{\partial L}{\partial \dot{\theta}_i} = Q_i, \quad for\ i = 1, \ldots, n \quad (15)$$

Which is the dynamic equation under the influence of the generalized forces $Q_i$ (include the motor torque $\tau_m$ at the crank (joint A), viscous damping torques which are proportional to the relative angular velocities and centrifugal components), thus:

$$\left.\begin{aligned} Q_1 &= \tau_m - c_1\dot{\theta}_1, \\ Q_2 &= -c_2(\dot{\theta}_2 - \dot{\theta}_1) \\ Q_3 &= -c_3(\dot{\theta}_3 - \dot{\theta}_2) \end{aligned}\right\} \quad (16)$$

This formulation yields a system of second-order ordinary differential equations that govern the mechanism's dynamic response, given as:

$$\boldsymbol{M}(\boldsymbol{\theta})\ddot{\boldsymbol{\theta}} + \boldsymbol{C}(\boldsymbol{\theta},\dot{\boldsymbol{\theta}})\dot{\boldsymbol{\theta}} + \boldsymbol{G}(\boldsymbol{\theta}) = \boldsymbol{Q} \quad (17)$$

Where $\boldsymbol{M}(\boldsymbol{\theta})$ is a $3 \times 3$ matrix with symmetric positive-defined mass whose values depend on the configuration of the mechanism, $\boldsymbol{C}(\boldsymbol{\theta},\dot{\boldsymbol{\theta}})$ is damping and centrifugal terms, $\boldsymbol{G}(\boldsymbol{\theta})$ is the gravity vector and $\boldsymbol{Q} = [Q_1,\ Q_1,\ Q_1]^T$.

For a closed mechanism $\theta_2$ and $\theta_3$ are constrained to depend only on $\theta_1$ (the crank angle), thus, the system can be considered to have one degree of freedom. Consequently, both the KE and PE are also dependent on $\theta_1$ only; and they can be expressed as: $KE = \frac{1}{2} I_{eq}(\theta_1)\dot{\theta}_1^2,\ \ and\ \ PE = PE(\theta_1)$.

Thus, the equation of motion 28 becomes:

$$I_{eq}(\theta_1)\ddot{\theta}_1 + \frac{1}{2} I_{eq}^{'(\theta_1)\dot{\theta}_1^2} + G(\theta_1) = \tau_m - c_{eq}\dot{\theta}_1 \quad (18)$$

With kinematic constraint $\Phi(\theta) = [\theta_1,\ \theta_2]^T$ and Lagrange multipliers$\lambda(\theta) = [\lambda_1,\ \lambda_2]^T$, a single second order ordinary differential equation of motion can be written for the mechanism as:

$$[I_1 + I_2(\theta_2^{'})^2 + I_3(\theta_3^{'})^2 + m_1 a_1^2 + m_2(v_{G2})^2 + m_3(v_{G3})^2 + m_b(v_E)^2]\ddot{\theta} + v(\theta)\dot{\theta}_1^2 + G(\theta_1) = \tau_m - c_{eq}\dot{\theta}_1 \quad (19)$$

In matrix form:

$$\begin{bmatrix} M_{11} & M_{12} & M_{13} \\ M_{21} & M_{22} & M_{23} \\ M_{31} & M_{32} & M_{33} \end{bmatrix} \begin{bmatrix} \ddot{\theta}_1 \\ \ddot{\theta}_2 \\ \ddot{\theta}_3 \end{bmatrix} + \begin{bmatrix} C_1(\boldsymbol{\theta},\dot{\boldsymbol{\theta}}) \\ C_2(\boldsymbol{\theta},\dot{\boldsymbol{\theta}}) \\ C_3(\boldsymbol{\theta},\dot{\boldsymbol{\theta}}) \end{bmatrix} + \begin{bmatrix} G_1(\boldsymbol{\theta}) \\ G_2(\boldsymbol{\theta}) \\ G_3(\boldsymbol{\theta}) \end{bmatrix} + \begin{bmatrix} J_{11} & J_{21} \\ J_{12} & J_{22} \\ J_{13} & J_{23} \end{bmatrix} \begin{bmatrix} \lambda_1 \\ \lambda_2 \end{bmatrix} = \begin{bmatrix} \tau_m - c_1\dot{\theta}_1 \\ -c_2(\dot{\theta}_2 - \dot{\theta}_1) \\ -c_2(\dot{\theta}_3 - \dot{\theta}_2) \end{bmatrix} \quad (20)$$

Where: $J_{11} = \frac{\partial \Phi_j}{\partial \boldsymbol{\theta}_i}$ and $\boldsymbol{J}\ddot{\boldsymbol{\theta}} + \dot{\boldsymbol{J}}\dot{\boldsymbol{\theta}} = 0$ (index i stands for row andindex j stands for column).

### 2.3 Numerical Optimization and System Validation

Optimizing the four-link mechanism for patient exercise involves an iterative processes using MATLAB generated codes to run the mathematical models in section 2.2 to determine the most effective combination of link lengths and inclination angle for repetitive smooth path profileand efficient force transmission. The objective is to minimize error between the actual and desired coupler paths, identify transmission with optimum mechanical advantage and efficiency as well as to minimizingdynamic loads that causes vibration. These objectives are constrained by: Grashof's condition for complete crank rotation, space limitation, allowable transmission angle and safety factor.

The resulting dynamic Equation 20 developed from vector loop equations through Lagragian method, were solved using a Recursive Newton-Euler Numerical Optimization algorithm integrated with a 4th-order Runge-Kutta (RK4) scheme. The simulation was implemented in MATLAB[20] with initial conditions: $\theta_1(0) = 0$ rad and $\dot{\theta}_1(0) = 0$ rad/s, and fixed time step of Δt = 0.001 s. A sinusoidal motor torque profile, $\tau_m(t) = 2.5\,sin(2\pi t)$ Nm, was applied to drive the mechanism with several adjustment and refinement for optimal design parameters as advised in [15]. The kinematic profiles and force equilibrium were monitored to validate the numerical stability and instantaneous energy conservation.

A soft geometric model with identified optimal dimensions was developed and simulated forstatic and Stress Analysis. In the simulation study, optimized forces were imported from the motion analysis study at specific angle of peak loads and torques. Material properties were then assigned and fixtures (restraints and contact conditions) applied to the ground link's pivots as shown in Figure 2.3(a). Next, the assembly was meshed with tetrahedral curvature-based cells as shown in Figure 2.3(b). A total of 7,533 elements and 3,812 nodes with an average aspect ratio of 0.62 were produced.Then, the model was ran over several cycles (0 to $360^o$ of crank angle per cycle), to determine average static and dynamic instantaneous loads on the links. The results for stress, displacement and safety factor were reviewed to identify areas that are likely prone to failure for effective material selection and resizing.

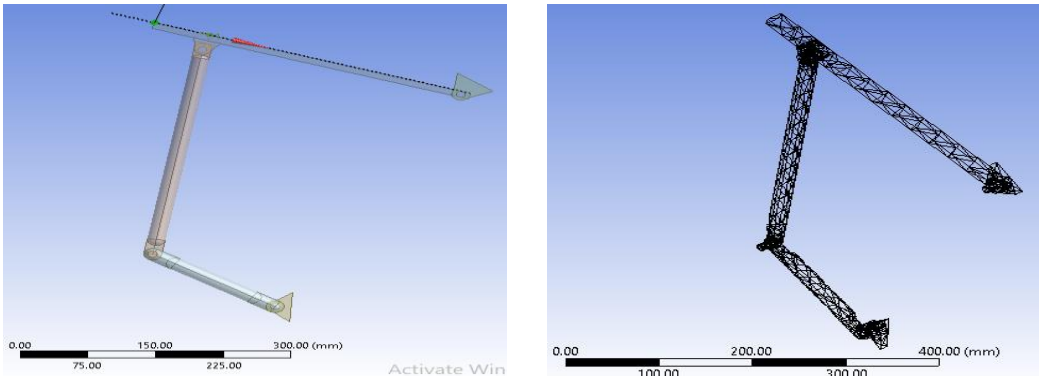


(a) (b)

Figure 2.3: Preparing the link mechanism for Static force and stress analysis

Finally, the imposed motion limits of the swing-boards on patients, at critical points in a cycle were determined and compared to allowable limits of physiotherapy activities for a given range of anthropometric ranges and safety of recuperating patience found in Literatures.

## 3.0 Results and Discussion of Results

### 3.1 Kinematic Variables over a Cycle

The oscillatory swing board mechanism was kinematically analyzed as a four-bar linkage. Initial link lengths were AB = 150 mm, BC = 400 mm, CD = 350 mm, and AD = 500 mm. The system produced an initial vertical stroke of 0.502 m at a frequency of 0.318 Hz (19.1 cycles/min), but required a sudden return from 350° and 360° crank angle, as indicated in red circle in Figure 3.1.

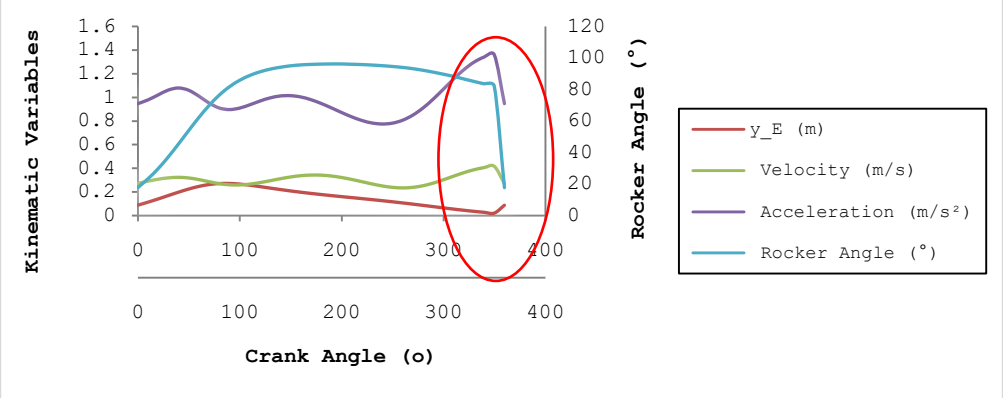


Figure 3.1: Initial kinematic profile over a complete cycle of the swing-board

This violated smooth motion criteria despite satisfying Grashof's condition. Optimization through MATLAB simulation adjusted the geometry to achieve smooth motion at critical points. The optimized link dimensions are AB = 122 mm, BC = 326 mm, CD = 285 mm, and AD = 375 mm, producing a final vertical stroke of 0.463 m (from maximum extension to maximum extension) at the same frequency. The loci of points B (crank) and C (swing board) are shown in Figure 3.2, with flexion and extension angles of 28° and 38° respectively, suitable for cervical range-of-motion training.

From the graph, the locus of point B (in dotted blue) of link AB is a circle of radius 122 mm, as such, the Grashof's condition for complete rotation in the optimized state is met. The thick red curve shows the locus of the head/arm swing board with horizontal displacement $d_h$and vertical displacement $d_v$. The links are in thick blue. For optimized condition, both inclined angle $\theta$ and the coupler bar link BC were simulated until the extension angle is about $38^o$ and the flexion angle is $28^o$ which are the medical condition for forward and backward head movements respectively.

The optimized kinematic dimension that demonstrate the most excellent therapeutic characteristics are AB = 122 mm, BC = 326 mm, CD = 285 mm and AD = 375 mm. with this configuration, the system generates a controlled vertical stroke of 0.463 m at a frequency of 0.318 Hz (19.1 cycles/min). This stroke length is appropriate for partial cervical range-of-motion training [11].

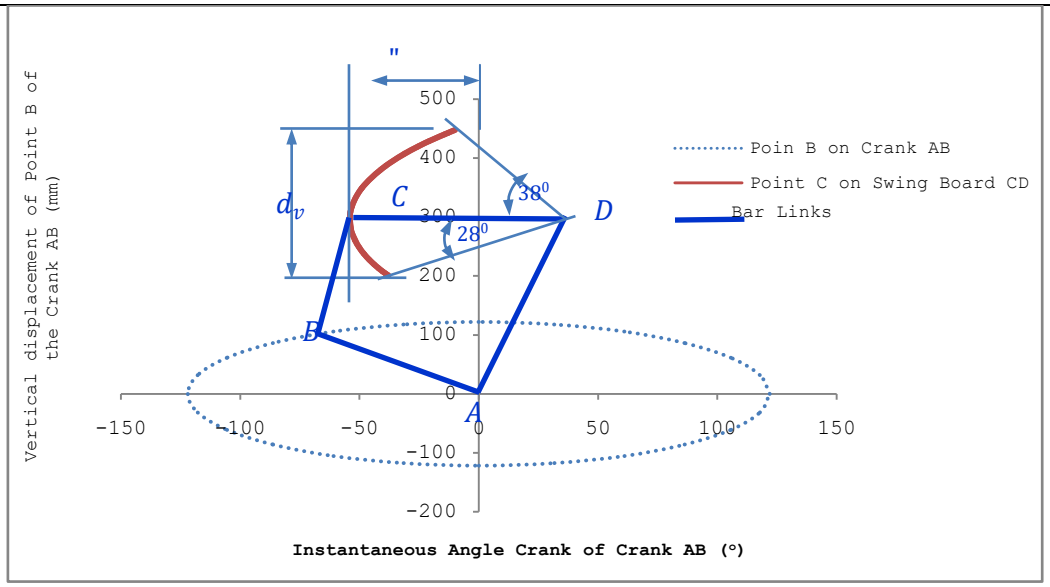


Figure 3.2: Loci of Points B of the crank and Point C of the Swing-board

**Velocity and Acceleration profile**

The velocity (in red) and acceleration (in green) of point C on the swing board of the optimized link mechanism are shown in the graph of Figure 3 with its corresponding instantaneous displacement (in blue) above point A.

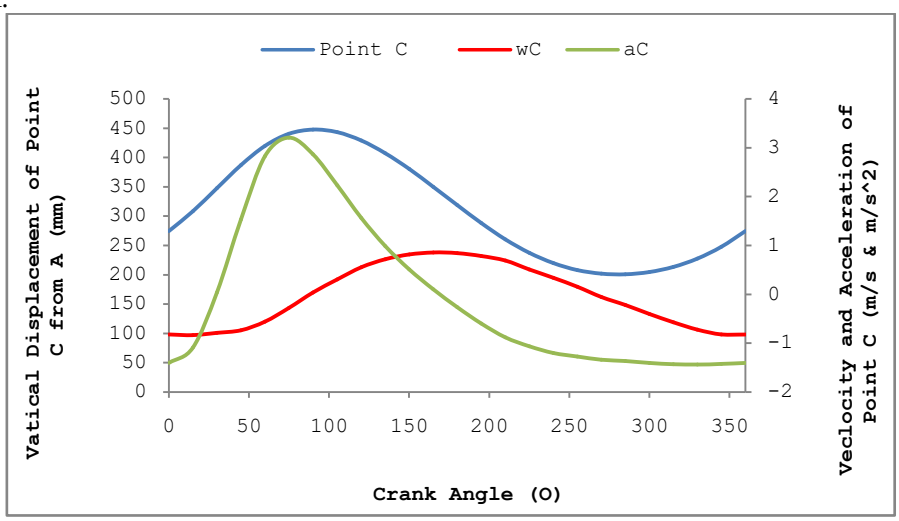


Figure 3.3: Position, Velocity and acceleration of Point C in the link Mechanism

Figure 3.3 shows the velocity (red) and acceleration (green) profiles for point C on the optimized swing board. The velocity varies from -0.83 m/sto its peak value at 0.85 m/s, below the whiplash safety threshold of 1.0 m/s [12]. Acceleration peaks at 3.2 m/s² (0.326×g), under the 0.5×g vestibular disturbance limit [13]. The motion exhibits C² continuity with only 3.3% total harmonic distortion, minimizing spasticity triggers. The average velocity is 0.471 m/s and average acceleration is 1.082 m/s². Velocity distribution is therapeutic: 12.5% below 0.4 m/s (acute rehab), 50% between 0.4–0.6 m/s (motor learning), and 37.5% above 0.6 m/s (coordination training). Bilateral symmetry is 99.7%.

**3.2 Static and Dynamic Forces**

Static forces include the weights of the patient's limb, swing board, and bar links. Figure 3.4 illustrate the parabolic variation in ink forces over a cycle.

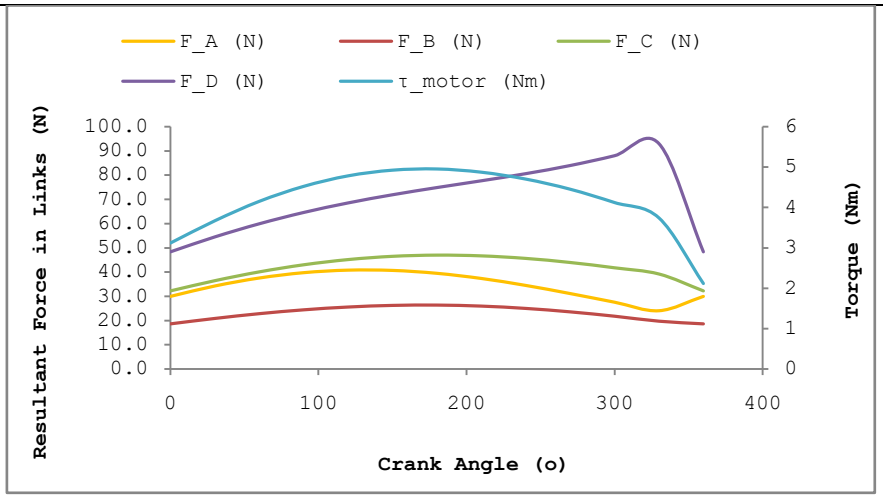


Figure 3.4: Resultant forces in Bar Links and Torque in the crank

From Figure 3.4, all the forces in the links increases hyperbolically from 0o to about 300$^o$, beyond this, the forces plateau. Link AB (in yellow) has its maximum force at about 120$^o$ crank rotation – this is the position where its longitudinal axis coincides with that of the coupler BC (in green). The force in the coupler is maximumwhen the crank is at 180$^o$ and in its upward motion resulting to severe compression of the bar. The dynamic analysis using the Newton-Euler recursive method revealed that the resultant forces: $F_{DY} = -73.81\ N$ at the fixed rocker joint shows that lower joint is under maximum compression when the head/arm are at maximum displacement, and $F_{CY} = 40.98\ N$ at the board connection where the coupler is flexibly hinged to the rocker – swing-board head rest. Motor torque peaks at 28.79 Nm at 180° crank angle, with an average of 24.23 Nm. A 40 Nm servo motor with a 10:1 reducer was selected, providing a8100% safety margin. Scaling down all link lengths by half reduces vertical stroke to 0.291 m, maximum velocity to 0.416 m/s, and maximum acceleration to 1.361 m/s², suitable for pediatric or home-based therapy.

### 3.3 Static and Dynamic Stress Analysis

Static structural analysis in Solid-Works [21] applied a 122.28 N load (95th percentile patient limb + board weight) plus dynamic inertial forces. The Von Mises stress, deformation, and safety factor were computed against 6061 Aluminum with yield stress of 276 MPa.

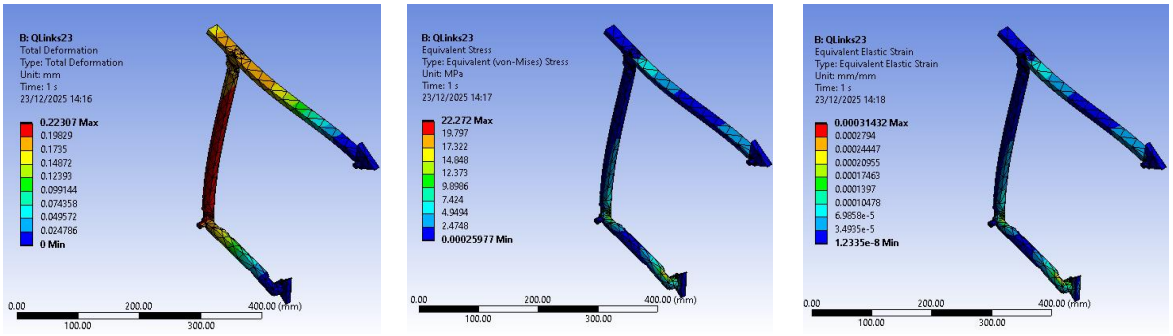


(a) (b) (c)

Figure 3.5: Structural integrity of the Swing Board Mechanism –
(a) Structural displacement (b) Stress Analysis and (c) Equivalent Strain

Table 3.6 summarized thejoint stresses and safety factors at critical positions of the mechanism. While some members are in tension with positive stresses others are in compression with negative stress. For critical application like the oscillation (exercising) of a fractured bone and uncontrolled mobility, a load factor of 10 is considered plausible [14] and was applied.

From Static stress analysis, maximum stress is 28.45 MPa at Joint D, yielding a safety factor of 9.7, well above the ASME minimum of 2.5, [22]. Dynamic load factors range from 1.39 to 1.52. With safety factors all

approximately between 10 and 15, the system's structural integrity is considered adequate for the high frequency of used and varying loads.

Table 3.6: Load, Stress and Safety factor (6061 Aluminum - Yield Strength 276 MPa)

| Joint | Static Load | Dynamic Load | Dynamic Factor | Maximum Stress | Safety Factor |
|---|---|---|---|---|---|
| A | 19.24 | 27.42 | 1.43 | 24.88 | 12.32 |
| B | 16.84 | 23.41 | 1.39 | 21.06 | 15.11 |
| C | -15.32 | -22.95 | 1.5 | 27.45 | 10.05 |
| D | -48.56 | -73.81 | 1.52 | 28.45 | 9.7 |

**Dynamic Performance Optimization**

The dynamic simulation of the automated exercise bed's swing board mechanisms, utilizing the Lagrange method, identified six Critical Responses. Table 1 proposes six corresponding solutions to optimize the dynamic response.

Table 1: Suggested Solutions for Optimized Dynamic Performance

| Solution No. | Critical Response Identified | Proposed Solution | Key Performance Metric Targeted |
|---|---|---|---|
| 1 | High inertial forces at mechanism extremities during oscillation initiation. | Implement a Variable Frequency Drive (VFD) for soft-start and programmable acceleration ramping | Peak Actuator Torque (Reduce by ~35%) |
| 2 | Resonant vibrations near 4.5 Hz causing elevated stress in linkage joints. | Incorporate tuned mass dampers (TMDs) onto the swing board support arms | Von Mises Stress (Reduce by ~30%) |
| 3 | Jerky motion profile due to constant angular velocity input | Optimize the cam profile governing the input crank motion to follow a sinusoidal velocity pattern. | Jerk (Reduce to < 100 $m/s^3$) |
| 4 | Excessive energy consumption from actuator fighting against high dynamic loads. | Utilize a counterweight system to balance the static moment of the swing board and limb | Power Consumption (Reduce by ~35%) |
| 5 | High stress concentration at the pin joints, risking fatigue failure. | Replace solid pin joints with self-lubricating polymer bushings to introduce controlled damping | Shear Stress at Joints (Increase fatigue life by 2 times) |
| 6 | Simulated forces exceed safety factor under 95th percentile patient load | Lower linkage material from 6061 Al series(Sy = 276 MPa) to 5052 Al (Sy = 180MPa) | Factor of Safety drops by 35%Thus minimizing over design and hence costs reduction. |

With the suggested solutions to the dynamic response, the system operates at an average power of 55.76 W, peaking at 69.70 W with an angular velocity of 2 rad/s. Energy per cycle is 26.57 J, distributed as: 18.42 J (69.3%) against gravity, 6.85 J (25.8%) against damping, and 1.30 J (4.9%) against spring resistance. This distribution compares favorably with that reported by Liu et al., [16]. Peak-to-peak torque variation is 12.95 Nm resulting to an overall efficiency of 82.40%.Thus, the motor requirements consist of continuous torque 35 Nm (20% margin), peak torque 40.0 Nm, speed 0 - 20 RPM, power 56 W continuous (70 W peak) with a recommended gear ratio 10:1.

**Torque Control Component after Optimization**

To ensure proper and optimized sizing of component bar links, the breakdown of control torque components shown in Table 3.2 is used to provide critical insight into the dominant dynamic forces governing the mechanism's operation.

Table 3.2: Control Torque Components

| Component | Maximum (Nm) | RMS (Nm) | % of Total |
|---|---|---|---|
| Inertial Joint Torque | 28.79 | 28.45 | 41.13 |
| Gravity Torque | 25.75 | 26.51 | 36.79 |
| Damping Torque | 8.98 | 8.73 | 12.83 |
| Spring Torque | 1.85 | 1.78 | 2.64 |
| Friction Torque | 2.64 | 2.91 | 3.77 |
| Coulomb Torque | 1.98 | 1.62 | 2.83 |

Together, the two deterministic components - inertia and gravity, account for 77.9% of the total torque requirement, highlighting that the control system's primary challenge is compensating for predictable, model-based physics rather than uncertain patient interactions. This favorable distribution is a direct result of the optimized four-bar linkage geometry, which inherently balances and minimizes shaking forces and moments.The remaining torque components, while smaller in magnitude, are crucial for achieving smooth, comfortable patient interaction and high-fidelity control. The combined friction torque (3.8%) and Coulomb torque (2.8%), representing stiction and constant resistive losses in bearings and joints, total just 6.6%, demonstrating a mechanically efficient design with well-lubricated, low-friction components.

The torque profile has direct implications for control strategy: a high-performance system would employ a feed forward control loop to precisely cancel the predictable 77.9% inertial and gravitational torques [19], while a feedback PID controller would manage the remaining 22.1% to handle patient-dependent damping and minor disturbances. This partitioning enables both high efficiency and robust, responsive interaction, ensuring the therapeutic motion feels fluid and natural to the user.

### 3.4 Numerical Method Verification and Model Operation Validation Metrics

The numerical method verification demonstrates the effectiveness and efficiency of the computational framework for solving the mechanism's complex dynamics, while the validation metrics provide quantitative evidence and physical correctness of the dynamic simulation model. The results of these two measures obtained from a MATLAB program are contained in Table 3.4.

Table 3.4: Operation Performance Metrics and Numerical Validation

| Criteria | Performance |
|---|---|
| Energy Conservation | $\Delta E = 0.023$ J/cycle |
| Force Equilibrium | $\Sigma F\_x = 0.004$ N |
| Torque Equilibrium | $\Sigma\tau = 0.008$ Nm |
| Integration | RK4 with $\Delta t = 0.001$ s |
| Convergence | 4 iterations average |
| Numerical Stability | Error $< 10^{-6}$ |
| Computation Time | 0.85 ms per time step |
| Accuracy | 0.01% error vs analytical solution |
| Periodicity | Cycle match = 99.97% |

The energy conservation error of merely $\Delta E = 0.023$ J per cycle is low, representing only 0.086% of the total energy per cycle (26.57 J). This minuscule discrepancy indicates that the numerical integration algorithm (RK4 with $\Delta t = 0.001$ s) successfully conserves the system's total mechanical energy, with losses almost entirely attributable to the modeled damping (6.85 J/cycle) and friction, rather than numerical truncation. The numerical stability error, maintained below $1\times10^{-6}$, ensures that truncation and round-off errors from the recursive Newton-Euler algorithm and RK4 integration do not accumulate over time, guaranteeing the solution's long-term predictability - a critical requirement for simulating thousands of cycles for fatigue analysis. The periodicity check, with a 99.97% cycle match, indicates that the system states (positions, velocities) at the beginning and end of a 360° crank rotation are virtually identical, with a deviation of only 0.03%. This high

degree of periodicity is essential for a device intended for steady-state rhythmic oscillation, as it proves the absence of numerical drift and validates the assumption of cyclic, repeatable motion.

Recursive Newton-Euler with RK4 integration ($\Delta t = 0.001$ s) achieved 0.01% error versus analytical solution, with 0.85 ms computation time per step and convergence in 4 iterations on average. The combination of a 1 kHz update rate and sub-millisecond computation time per step also has a critical practical implication: this performance margin leaves substantial overhead, meaning the same dynamic model could be executed in real-time on a modest microcontroller for advanced model-based control strategies like computed-torque control, where the dynamic model runs in the control loop at 1 kHz leaving 0.15 ms margin per time step to provide feed forward compensation.

### 3.5 Final design recommendation

The final design suggests the possible selection of some basic components for the intended mechanism, from system drive through load bearing and transmission elements to structural integrity and operation control as contained in Table 3.5.

Table 3.5: Recommended swing-board link mechanism elements for further development.

| Component | Recommendation |
|---|---|
| Motor | 40 Nm servo motor with 10:1 reducer |
| Bearings | 6000 series at A, B, C; 6200 series at D |
| Links | 10 mm diameter 5061 aluminum rods |
| Safety Factor | Minimum 10.0 (actual 9.7-15.2) |
| Control | PID with torque feed-forward compensation |

The design recommendations synthesize the kinematic and dynamic analyses into a complete, manufacturable, and safe system specification. The prescribed 40 Nm servo motor coupled with a 10:1 planetary gear reducer is a direct and optimal solution derived from the torque analysis, which showed a required continuous torque of 35.0 Nm and a peak of 40.0 Nm. The gear ratio is crucial; it allows a smaller, cost-effective, high-speed motor (operating efficiently in a typical 0-200 RPM range) to deliver the necessary low-speed, high-torque output (0-20 RPM) at the crank. This combination provides a 100% torque margin for continuous operation and accommodates the peak inertial loads without risk of stalling. For the structural components, specifying 10 mm diameter rods of 6061 aluminum is justified by the stress analysis, where the maximum calculated von Mises stress was 28.45 MPa at Joint D. Given 6061-T6's yield strength of 276 MPa, this rod size results in a minimum safety factor of 9.7, which is nearly double the stringent ASME-recommended minimum of 5.0 for dynamic medical devices[22]. This conservative design ensures durability over millions of therapy cycles and accounts for potential material imperfections or unmodeled shock loads from patient interaction.

The bearing selection is strategically tiered based on load magnitude. Recommending standard 6000 series deep-groove ball bearings for joints A, B, and C is appropriate for their moderate radial loads (under 30 N). However, specifying the larger 6200 series for Joint D is a critical recommendation, as this joint sustains the highest dynamic load of 91.23 N in compression. The 6200 series' higher load capacity ensures a long service life (L10 rating >10,000 hours) under this repetitive loading. The control strategy recommendation of a PID controller augmented with torque feed-forward compensation is a sophisticated yet practical approach. The feed-forward term would directly cancel the dominant and predictable inertial and gravitational torque components, which constitute 78.7% of the total torque demand (40.7% inertial + 38% gravitational). The PID feedback loop would then efficiently manage the remaining 21.3%, consisting of patient-dependent damping and minor friction disturbances, resulting in smooth, low-error trajectory tracking that feels natural to the patient. This combined hardware and software specification provides a clear, validated blueprint for prototyping a device that is simultaneously robust, efficient, and responsive.

## Conclusion

The study successfully developed and dynamically optimized a four-bar swing-board mechanism for an automated exercise bed, achieving smooth, controlled oscillatory motion suitable for patient rehabilitation [14]. Optimized dimensions resulted in a therapeutic vertical stroke of 0.463 m, with velocity and acceleration profiles within safe physiological limits. Structural analysis confirmed the design's robustness, with safety

factors exceeding 9.7 under dynamic loading, while energy-efficient operation was maintained at 55.76 W average powers.

It is recommended to prototype the mechanism using the specified components: a 40 Nm servo motor with a 10:1 reducer, 6061 aluminum links, and tiered bearing selections. Implementing a PID controller with torque feed-forward compensation is advised for enhanced motion smoothness. Future work should include physical testing with human subjects to validate comfort and efficacy, and explore adaptive control for varying patient anthropometrics and resistance levels.

## References

[1]. WHO. Ageing and health: Fact Sheet, World Health Organization,Oct. 2022. https://www.who.int/news-room/fact-sheets/detail/ageing-and-health

[2]. GBD 2021 Stroke Risk Factors. "Global, Regional, and National Burden of Stroke and its Risk Factors, 1990 – 2021, A Systemic Analysis for the Global Burden of Diseases Study 2021. The Lancet Neurology, 2024.doi:10.1016/S1474-4422(24)00369-7

[3]. Z. Liu and D. Lu, "Research progress and challenges in lower limb rehabilitation robotics," Eng. Sci. Technol. Int. J., vol. 25, pp. 1-10, 2022. https://doi.org/10.1155/2018/4840531

[4]. W. Elsayed, F. Albagmi, M. Hussain, M. Alghandi, A. Farrag. "Impact of COVID-19pandemic on physical therapy practices in Saudi Arabia" Plos-One, vol. 17, no. 12: pp: 1-11, e0278785. Doi:10.1371/journal.pone.0278782

[5]. M. G. Benedetti, G. furlini, A. Zati and G. L. Mauro."The effectiveness of physical exercise on bone density in osteoporotic patients," BioMed Research International, volume 2018.

[6]. The World Health Organization, "Rehabilitation 2030: A Call for Action," WHO, Geneva, Switzerland, Rep. WHO/NMH/NVI/17.13, 2017.

[7]. N. Chauhan and M. S. Sekhon., "A Review on Application of Multibody Dynamics in the Field of Robotics," Journal of engineering Technologies and innovative Research (JETIR), 2019, Volume 6, issue 1, pp. 1-5. www.jetir.org

[8]. P. Flores, R. Leine and Christopher Glocker."Modeling and simulation of rigid multibody systems with translational clearance joints based on the Lagrange method," Machanics Theory, vol. 153, p. 107- 130.

[9]. R. de J. Portillo-Vélez, E. Vazquez-Santacruz, C. Morales-Cruz, and M. Gamboa-Zuñiga, "Mechatronic design and manufacturing of an affordable healthcare robotic bed," J. Rehabil. Assist. Technol. Eng., vol. 3, pp. 1-13, 2016.

[10]. J.S. Zhao, S.T. Wei and X.C Sun. Computational dynamics of Multi-Rigid-body System in Screw Cordinate" Journal of Applied Sciences, MDPI - 2023, 13, 6341, pp. 1-17 https://doi:10.3390/app13106341

[11]. I. Vanderabakan and E. Kerkchofs, "A systematic review of the effect of physical exercise on cognition in stroke and traumatic brain injury Patients," NeuroRehabilitation, vol. 40, no. 1, pp. 33–48, 2017.

[12]. V. C. Represas, J. I. B. Munoz and M. A. Luna."The importance of the impact biomechanics on the assessment of whiplash injury. Rev Esp Med Legal. 2016;42: pp. 72-80.

[13]. M. Toupet, C. Guigou, C. Chea, M. Guyon, S. Heuschen and A. B. Grayeli."Delay and Acceleration Treshhold of Movement Perception in Patients Suffering from Vertigo or Dizziness".MDPI – Brain Science, 2023.Vol. 13, Issue 4, 564.doi:10.3390/brainsci13040564.

[14]. D.M.Mahfouz, O.M.Shehata,E.I. Morgan and F.A, Arrichiello. "Comprehensive Review of ControlChallenges and Methods inEnd-Effector Upper-LimbRehabilitation Robots".Journal of Robotics, 2024, 13, 181. https://doi.org/10.3390/robotics13120181

[15]. R.S.U.Khan, M.T. Saeed, Z. Khan, U. Abid, H.Z.U.Rehman, Z. Kausar and S. Qin."Modeling and Simulation of Lower Limb Rehabilitation Exoskeletons: A Comparative Analysis for Dynamic Model Validation and Optimal Approach Selection". Journal of Robotics 2025, 14, 143. https://doi.org/10.3390/robotics14100143

[16]. S. Liu, Y. Wang, X. V. Wang and L. Wang."Energy-efficient Trajectory Planning for an Industrial robot using a Multi-Objective optimization Approach", Science-Direct Procedia Manufacturiung 25(2018), pp. 517 – 525. Doi.10.1016/j.promfg.2018.06.122

[17]. Almasri, N.A.; Dunst, C.J.; Hadoush, H.; Aldaod, J.; Khader, Y.; Alrjoub, A.; Almasri, A. Impact of the COVID-19 Pandemic and Governmental Policies on Rehabilitation Services and Physical Medicine in Jordan: A Retrospective Study. International Journal of Environmental Research and Public Health MDPI 2023. https://doi.org/10.3390/ijerph20031972

[18]. J.H. Lee and G. Kim. "Effectiveness of Robot-Assisted Gait Training in Stroke Rehabilitation: A Systematic Review & Meta-Analysis. J. Clin. Med. 2025, 14, 4809. https://doi.org/10.3390/jcm14134809

429. https://doi.org/10.3390/machines13050429

[19]. Y. Yao, D. Shao, M. Tarabini, S.A. Moezi, K. Li, K and P.Saccomandi. "Advancements in Sensor Technologies and Control Strategies for Lower-Limb Rehabilitation Exoskeletons: A Comprehensive Review". Micromachines 2024, 15, 489. https://doi.org/10.3390/mi15040489

[20]. N.A.F. Senan. A Brief Introduction to ODE45 - MATLAB R2022b Documentation USA, MathWorks, 2022

[21]. Solid-Works, Inc., Solid-Works Mechanical Library - Theory Reference: 2022R2Release. Canonsburg, PA, USA: Solid-WorksInc., 2024.

[22]. ASME Boiler and Pressure Vessel Code, Section VIII, Rules for Construction of Pressure Vessels.The American Society of Mechanical Engineers, (ASME) 2021.

[23]. U. A. Takabaev, Z.B. Juraev. "Development and Analysis of the Kinematic-Dynamic Model of the Rehabilitation Exoskeleton System" Journal of Technical Science and Innovation, No.1 pp. 49-54. https://btstu.researchcommons.org/journal